INTERNATIONAL JOURNAL OF ADVANCED ENGINEERING AND BUSINESS SCIENCES (IJAEBS)

Journal homepage: https://ijaebs.journals.ekb.eg

Experimental Assessment of Progressive Collapse of Reinforced Concrete Beam-Column Assemblages

F.B.A. Beshara[a], Ahmed. A. Mahmoud[*b] Osama O. El-Mahdy[c], and Ahmed N. Khater[d]

a Associate Professor, Department of civil engineering, faculty of engineering (Shoubra), Benha University,108 Shoubra St., Shoubra, Cairo, Egypt

b Professor of Reinforced Concrete Structures, Department of civil engineering, faculty of engineering (Shoubra), Benha University,108 Shoubra St., Shoubra, Cairo, Egypt

c Professor of Structures, Department of civil engineering, faculty of engineering (Shoubra), Benha University,108 Shoubra St., Shoubra, Cairo, Egypt

d Assistance Professor, Department of civil engineering, faculty of engineering (Shoubra), Benha University,108 Shoubra St., Shoubra, Cairo, Egypt

**Corresponding author*: Email address: ahmed.m5882@gmail.com

Received: 24-09-2022 **Accepted:** 13-11-2022 **Published**: 05-06-2023

ABSTRACT

This paper introduces the experimental program implemented to study the load-carrying capacity of seven reinforced concrete beam-column assemblages under monotonic vertical load against progressive collapse due to removal of the interior column. The specimens were designed and detailed according to the Egyptian code provisions. The specimens were one-quarter of the full scale and designed with and without seismic detailing to verify the effect of reinforcement detailing and flanges on the assemblage structural behavior. Each specimen represented a two-consecutive beam spans subsequent to the elimination of the first story interior column. In all assemblages, the external two columns were restrained against the vertical and the horizontal deformations and loads were applied monotonically at the top of the interior column stub. For each load step, the results of mid-span deflection, concrete strains, reinforcing steel strains, and load capacities were documented. The tests showed that the compressive arch action (CAA) improve the beam-column assemblage flexural capacity. The arching capacity was noticed to be a function of the longitudinal reinforcement ratios, seismic and non-seismic detailing, and the

existence of concrete flanges. The response of the beam-column assemblages is evaluated through determinations of the displacement ductility level, the amount of absorbed energy, the contribution of the compression arching action, and activation of the catenary action. The test results are validated by two existing theoretical models through the calculations of the assemblage peak capacity.

Keywords: Experimental Assessment; Progressive Collapse; Reinforced Concrete; Beam-Column Assemblages.

1 INTRODUCTION

With the increase of terrorist attacks against the important governmental and commercial buildings, which are frequented by a large number of citizens, it was imperative for the researchers to develop design methods that enable the buildings to face these attacks. The best methods to evaluate the safety of buildings is the ability of the structure to prevent a complete collapse after the loss of one load bearing element due to any abnormal events. During the previous decades, various reasons have signified the importance of mitigation in contradiction of progressive collapse to the engineering design organizations. Subsequently, modifications in the building codes have been presented to report the probability of progressive collapse. One of the best comprehensive definitions for the progressive collapse has been given through ASCE 7-10 specifications [1], "The progressive collapse is the spread of local failure from structural element to another, leading to complete failure of the building or parts of it". Theoretically and analytically, the cause of the progressive collapse is a change of structural elements boundary conditions so that they carry more loads than their loading capacity and, then the collapse spread along with all building elements. According to [2, 3], there are more than one method to ensure reducing the effect of the progressive collapse in buildings. The first of these methods is called event control by preventing the causes of external collapse through barriers surrounding the buildings. The second strategy called the direct method, which is based on the structural analysis of the buildings, taking into account the ability of the structure to face any abnormal hazards at the design stage. The third method called the indirect method, which is not based on the computational analysis of the structures to deal with abnormal hazards, but rather, a guarantee a minimum quantity of links between typical structural elements. Resistive and reasonable design to resist successive collapses of buildings must include a combination of direct and indirect design methods to strengthen the different building elements, and thus utilization of the benefits from each method.

Several experiments have been performed on the beam–column assemblages to investigate the effect of different variables in resisting the progressive collapse. Farhang et al. [4] carried out laboratory tests for six specimens representing 40 % of the actual scale. The basic variables studied were the ratios of top and bottom reinforcing steel bars as well as the distribution of stirrups along the length of the beam. The results show that increases the ratios of longitudinal reinforcement led to an increase in the maximum load capacity for beam-column assemblages, the good distribution of the shear links at the full length of the beam leads to prevent the occurrence of brittle shear failure and enhance the maximum loading capacity of the assemblages.

Yu et al. [5] conducted laboratory tests on six specimens, which consists of double bay beams and two exterior columns at the ends of the beam-span. The selected specimens represent 50% of the actual scale. The study concluded that compression arch action significantly enhances the structural resistance of the beam-column assemblages with lesser span-depth proportions, the participation and contribution of catenary action in strengthening structural resistance with increasing the reinforcing steel ratio and span-depth ratios.

In another study by Tsai et al. [6], it was concluded that increasing the distance between stirrups leads to reduce compression arch action and catenary action, the increase of beam span-to-depth ratio leads to an increase in the catenary action stage and decrease in compression arch action stage.

Pour et al. [7] found that increasing the assemblage concrete compressive strength leads to an increase in the peak load capacity of the tested assemblages, increasing longitudinal reinforcement ratios have a great ability to improve and enhance assemblage peak load carrying capacity.

Chanh et al. [8] conducted laboratory tests on four specimens demonstrating the beam-column assemblages with seismic and non-seismic details provisions. The selected specimens represent 35% of the actual scale. The study concluded that using of reinforced concrete moment resisting frames in the design of the buildings in addition to seismic detailing led to considerable load carrying capacity in contradiction of successive collapse introduced by abrupt loss of column support.

The previous experimental studies [4–8] neglected the effect of concrete slabs on the resistance of progressive collapse. Ren et al. [9] and Lu et al. [10] conducted experimental tests on beam-column specimens with considering the contribution of the slabs. Their test outcomes showed that the hazard of collapse can be extensively reduced by the addition of slabs.

This paper shows a complete description of the experimental program that was developed to study the behavior of beam-column assemblage designed in accordance to Egyptian Building Code [11 and 12] which is similar to American Code [13]. The assemblages are exposed to an interior column removal scenario, where the column removal is resulting in increasing deflections, doubling of beam spans, and increasing of beam downward loads. The formation of flexural action, compressive arch action, and catenary action mechanisms are studied. These features are away from the provisions of the usual design and may result in failure of buildings. The main studied parameters of the assemblages are:

(a) Different ways of reinforcing detailing techniques;

(b) The influence of the bottom and the top reinforcement ratios;

(c) The flanges contributions for seismic and non-seismic detailing, and

(d) The effect of the bottom reinforcement lap splices.

2 EXPERIMENTAL PROGRAM

2.1 Design of Specimens

The prototype of test specimens is supposed to be placed at the center of a multi-bay interior frame. The interior frame is included in an 8-story commercial building in Cairo, of which the ground story is 4.50 m height and a typical story height of 3.30 m high. The distances between columns are 4.40 in the two perpendicular directions. The live load is 3.00 kN/m^2, the floor cover is 1.50 kN/m^2, the slab thickness is 0.12m, and the equivalent load of walls is 2.16 kN/m^2. The service dead and live load on the interior frames are 23.1 kN/m` and 9.60 kN/m`, respectively. The seismic lateral loads considered in this study are as per Egyptian Code ECP 201-2012 [12]. The soil type is composed of dense sand that means soil class is C. The commercial building is considered to be in seismic zone 3, with design ground acceleration ag = 0.15 g. The building is designed as a moment-resisting frame with a base shear coefficient of 5.0 in the two perpendicular directions. In the design of prototype building elements, a concrete compressive strength of 35 MPa and a reinforcing steel yielding strength of 400 MPa were considered. The column section of the prototype structure was 800 x 800 mm and the longitudinal reinforcement ratio ρl = 1.0%. The beam section was 250 x 1000 mm. The design of frames is based on seismic and non-seismic design as per the Egyptian Code of practice ECP 203-2017 [11].

In order to study the effect of progressive collapse on beam-column assemblages, an interior column was removed. After the elimination of the central column as presented in Fig. 1, the shaded segment of the interior frame became the most critical part in the entire building due to

the fact of doubling of the distance between columns and intensified gravity loads. Assuming no failure in the two columns adjacent to the eliminated one according to the progressive collapse design codes [2 and 3], and appropriate lateral restraint stiffness for the residual building. Seven specimens were designed, the specimens had similar concrete dimensions and varied reinforcement ratios. The assemblage was scaled to 25 % of the prototype structure, representing two consecutive beam spans subsequent to the elimination of the first story central column. As shown in Fig. 2, the beams dimensions are 120 mm width and 250 mm in depth. The span-to-depth ratio is 8.0 with a clear span length equal to 2000 mm. The column dimensions are 200 mm square section. The specimens are designated as S1, S2, S3, S4, S5, S6, and S7. Details of the longitudinal reinforcement configurations and stirrups are given in Table 1. The design of the specimens from S1 to S4 represents the non-seismic design, while the specimens from S5 to S7 stand seismic design and detailing. Compared with the gravity loads design, usually, the seismic design needs higher longitudinal and shear reinforcement ratios to withstand lateral shear forces. To take into account the continuation effect of beams in the prototype structure, the longitudinal bars were anchored to the columns with the tail extension of the hook.

For non-seismic specimens group, Fig. 3 shows the rebars placements of specimens S1. The top reinforcement ratio at the central and at the beam-ends is 0.52% (2ϕ10). The stirrups are distributed at 100 mm on the beam span and the top reinforcement is curtailed at specified positions as shown in Fig. 3. The bottom reinforcement ratio is 0.52 % (2ϕ10), with lap splice. S2 is the same as S1 but with the addition of the top flanges. In order to study the effect of top reinforcement ratios on the assemblage behavior, specimen S3 top reinforcement ratio is increased at the middle and at the beam-ends from 0.52% to 0.75% (2ϕ12). Specimen S4 is the same as specimen S1 but the bottom reinforcement ratio is changed from 0.52% (2ϕ10) to 0.75% (2ϕ12). For the seismic detailing specimens group, the assemblage S5 is the control specimen. Figure 4 shows the reinforcement curtailments of specimens S5. The top reinforcement ratio at the central and the beam-ends is 0.75% (2ϕ12). The stirrups are distributed at 50 mm on the beam span, and the bottom reinforcement ratio is 0.52% (2ϕ10). The bottom rebars of specimen S5 are lap spliced at a distance of (2d) from the interior column. The bottom reinforcement of the specimen S6 is continuous through the two adjacent beam spans and has no lap splice at the interior column zone. Specimen S7 is the same as the specimen S5 but with the addition of the flanges.

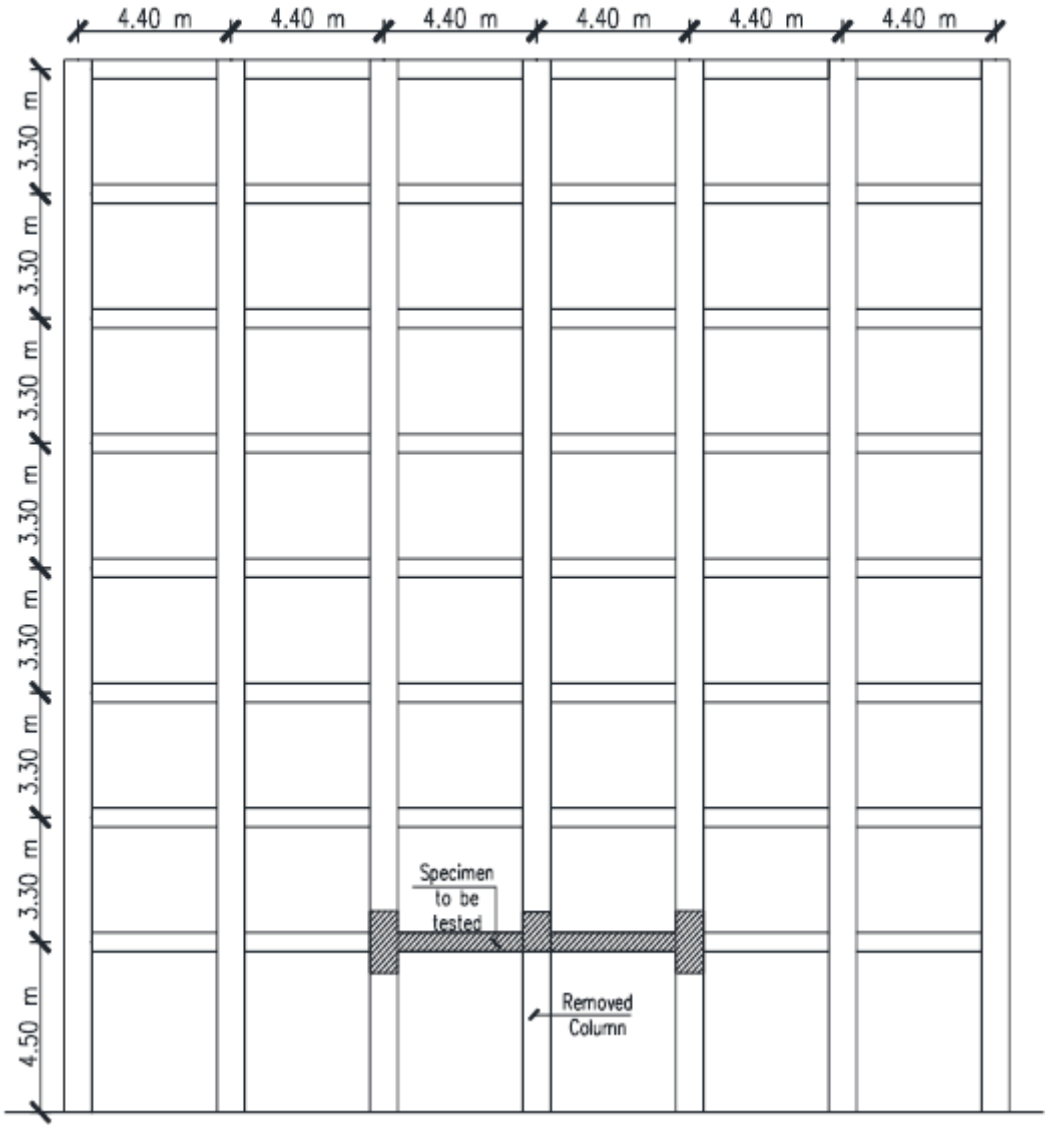

Figure 1: Commercial building elevation.

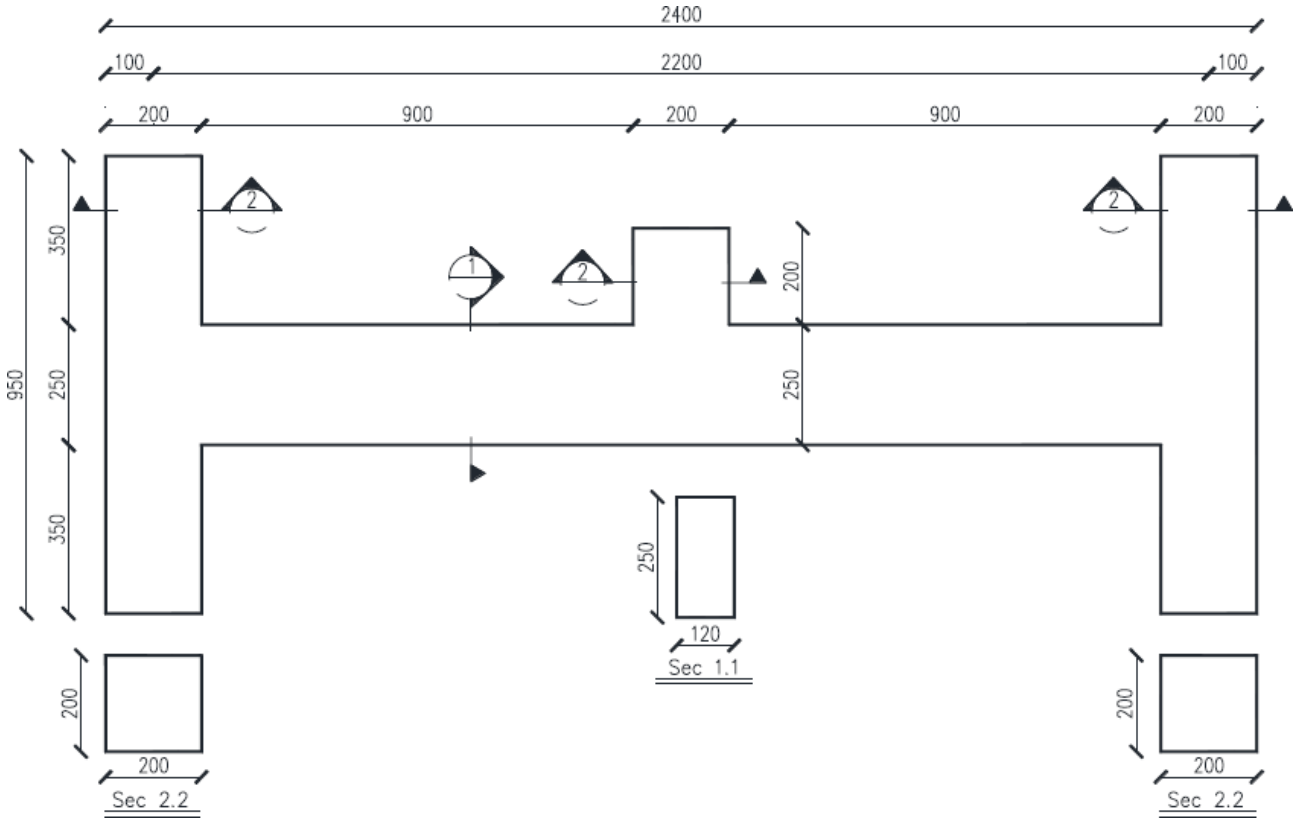

Figure 2: Specimen concrete dimensions (Dimensions in mm).

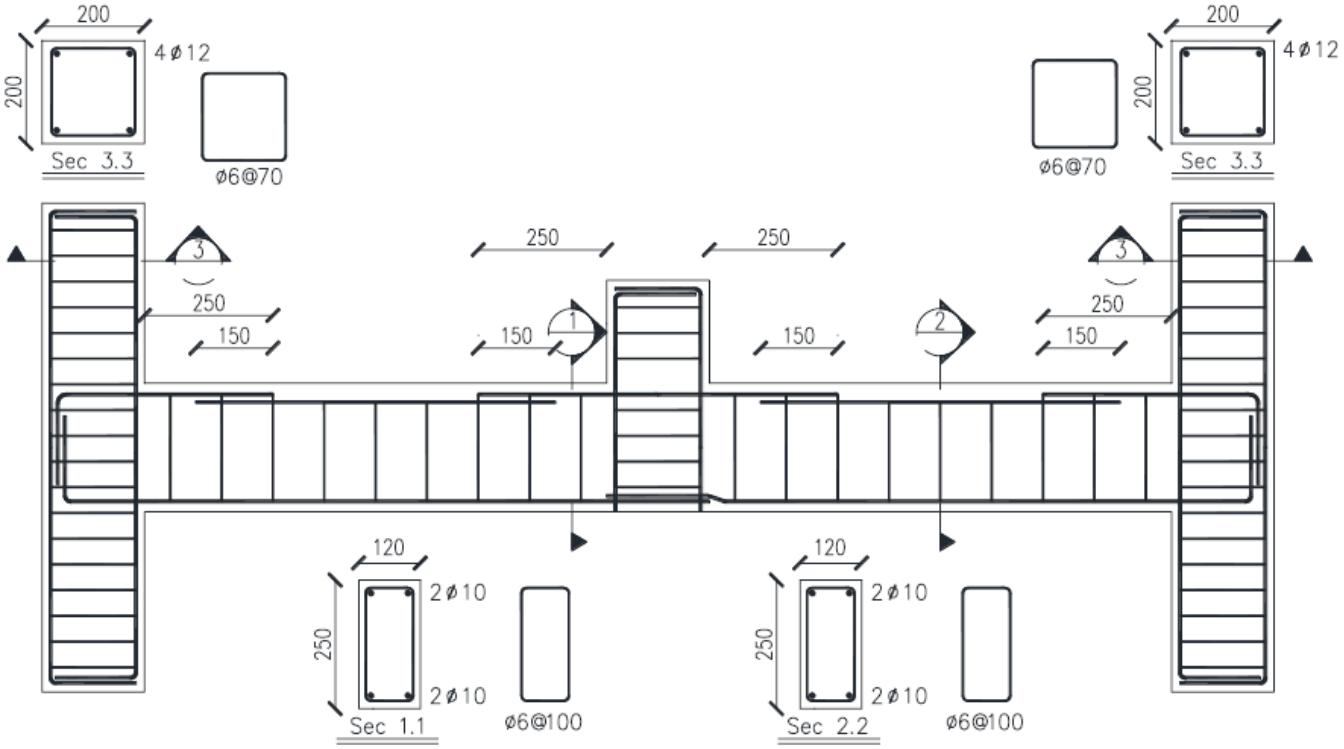

Figure 3: Reinforcement details of specimen S1.

(Non-Seismic Detailing).

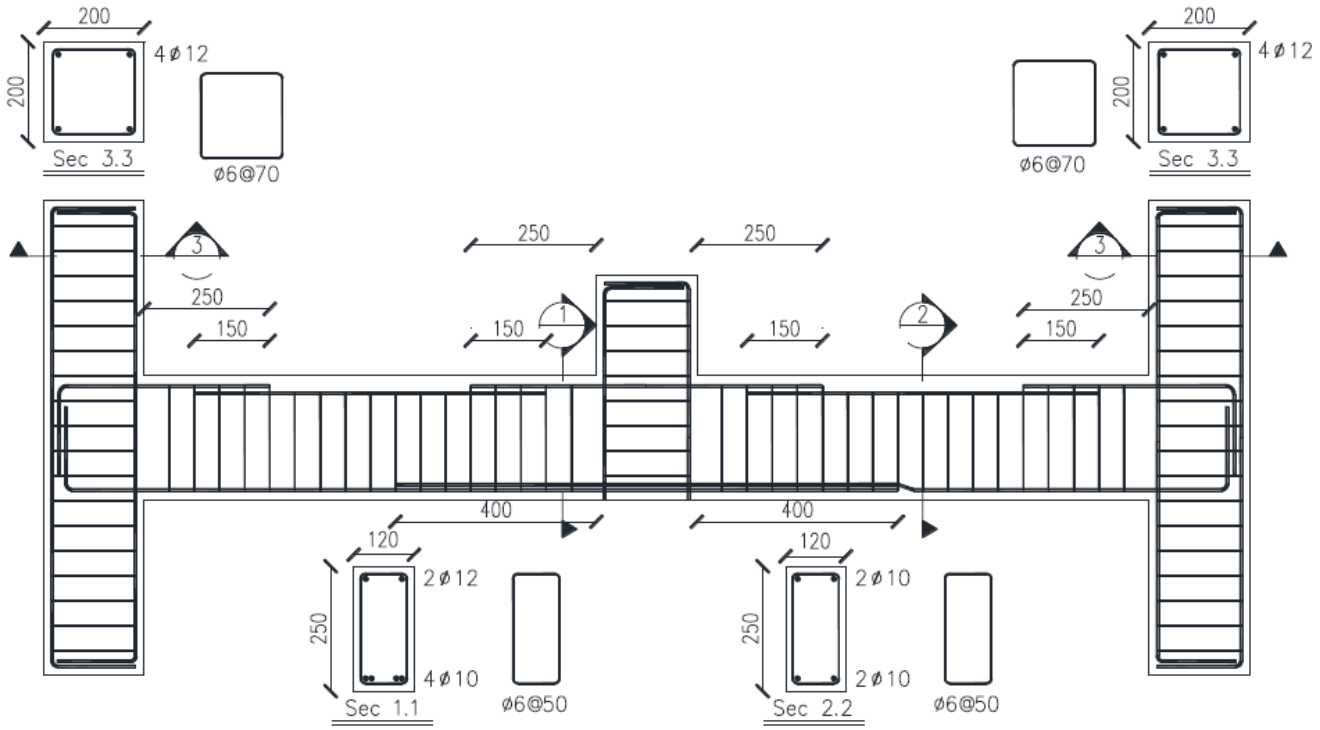

Figure 4: Reinforcement details of specimen S5. (Seismic Detailing).

Table 1: Details of beam-column assemblages specimens.

Specimen No.	Width (*b*) (mm)	Height (*h*) (mm)	Slab Thickness (t_s) mm	Slab width (B) (mm)	Longitudinal Reinforcement (ρ_l)				Beam Stirrups	Concrete compressive strength (MPa)
					Section 1-1 Mid Span		Section 2-2 Beside Columns			
					Top (ρ_l %)	Bottom (ρ_l %)	Top (ρ_l %)	Bottom (ρ_l %)		
S1	120	250	---	---	2 Φ 10 (0.52%)	2 Φ 10 (0.52%)	2 Φ 10 (0.52%)	2 Φ 10 (0.52%)	Φ6@100	41.20
S2	120	250	70	540	2 Φ 10 (0.52%)	2 Φ 10 (0.52%)	2 Φ 10 (0.52%)	2 Φ 10 (0.52%)	Φ6@100	42.45
S3	120	250	---	---	2 Φ 12 (0.75%)	2 Φ 10 (0.52%)	2 Φ 12 (0.75%)	2 Φ 10 (0.52%)	Φ6@100	41.20
S4	120	250	---	---	2 Φ 10 (0.52%)	2 Φ 12 (0.75%)	2 Φ 10 (0.52%)	2 Φ 12 (0.75%)	Φ6@100	42.45
S5	120	250	---	---	2 Φ 12 (0.75%)	4 Φ 10 (1.04%)	2 Φ 12 (0.75%)	2 Φ 10 (0.52%)	Φ6@50	43.15
S6	120	250	---	---	2 Φ 12 (0.75%)	2 Φ 10 (0.52%)	2 Φ 12 (0.75%)	2 Φ 10 (0.52%)	Φ6@50	43.75
S7	120	250	70	540	2 Φ 12 (0.75%)	4 Φ 10 (1.04%)	2 Φ 12 (0.75%)	2 Φ 10 (0.52%)	Φ6@50	43.15

Where: $\rho_l = As/(b*h) *100$; A_s is the area of steel reinforcement ; $B= 6\ t_s + b$

2.2 Material Properties

Experimental tests were performed in order to maintain the mechanical properties of both concrete and steel reinforcement. For each concrete patch, six standard cubes (1500 mm) were arranged for determination of the concrete compressive strength. Table 1 shows the results of the testing cubes for all specimens. High tensile deformed steel bars with diameters of 10 and 12 mm were used for the longitudinal reinforcement in the beam-column assemblages, and mild steel round bars with 6 mm diameter were used for stirrups. Tensile tests were conducted on sample of reinforcing bars to determine their true mechanical tensile properties. Table 2 lists the measured tensile properties of the used bars during the experimental tests.

Table 2: Properties of reinforcing steel bars.

Diameter (mm)	Type	Yield Strength (N/mm^2)	Ultimate Strength (N/mm^2)	Elongation (%)
6	Mild steel	323	478	28.8
10	High Tensile Steel H.T.S	498	762	19.4
12	High Tensile Steel H.T.S	516	785	17.1

2.3 Test Set-Up and Procedure

Figure 5 shows a schematic drawing of the reinforced concrete assemblage test setup. The upper and the lower parts of the exterior columns were connected to the steel frame by using two plates and four rods in order to prevent it from the possible out of plane horizontal deformations. LVDT1 is used for measuring the assemblage middle displacement and was at a distance of 1000 mm from the face of the exterior column. LVDT2 is used to record the assemblage vertical deformation at each quarter of the beam span. A load cell with capacity of 500 kN was attached to the reaction beam with a hydraulic jack to apply the load at the top of the interior column stub. The assemblages were examined under displacement control technique. The vertical displacement rate was chosen to be 0.25 to 0.75 mm per minute. At the end of each increment stage, the cracks propagations were recorded and marked through the beam spans and exterior columns. A 20 mm thick loading steel plate was added to the upper part of the central column in order to guarantee a full distribution of applied loads and preventing local stresses concentrations.

If the mid-span deflection reached 50 mm, the loading frequency was doubled by increasing the applying loads increments. When the beam mid-span deflections touched the limit of 160 mm,

the test might be stopped, because of lab restrictions and safety requirements. The Demec points and dial gauges were used to record the concrete strains. The points were fixed at the top and the bottom part of the assemblage mid-span. In order to shed light on the beam internal forces, electrical strain gauges were connected to the longitudinal reinforcing bars at different positions. Two electrical strain gauges were used for each specimen at the mid-span bottom reinforcement and at the end-span top bars. The properties of the used electrical strain gauges were as follows; 6 mm gauge length, 2.12-gauge factor, and 120.3 ± 0.5-ohm gauge resistance. The load cell, electrical strains gauges, and LVDTs were attached to a data logger system in order to record all results through the test stages.

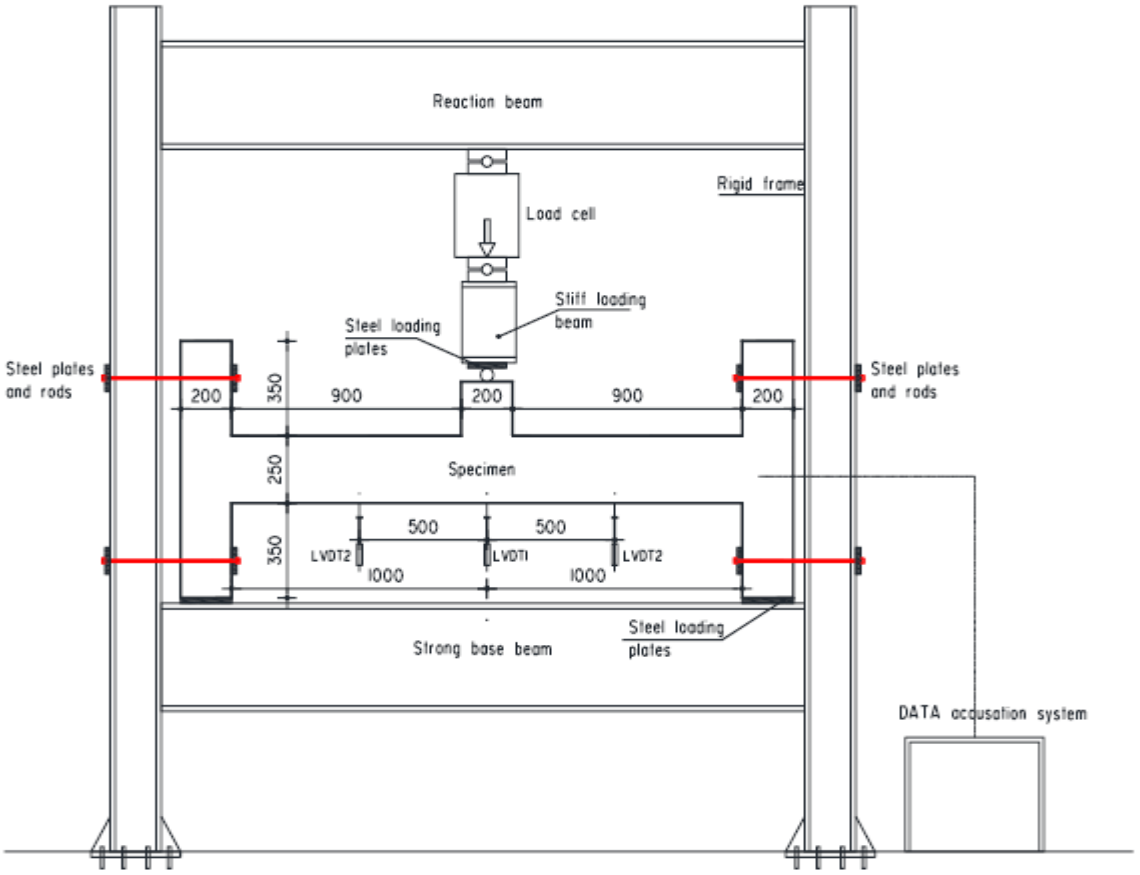

Figure 5: Schematic of the test setup.

3 EXPERIMENTAL RESULTS

3.1 Observed Behavior and Failure Modes of Non-Seismic Specimens

The general behaviour and failure modes of the testing specimens are illustrated based on the observed crack patterns propagation under the applied load through the tests. The crack patterns process are divided into two phases. The first one is the compression arch action phase where the cracks fundamentally initiated by bending moments since the cracks spread orthogonal to the beam axis and ended at the beam neutral axes. The second phase is the catenary action which took place after the crushing of concrete, so the reinforcement and part of the specimen are subjected to direct tensile force. Throughout the catenary phase, cracks are almost regularly extended all over the beam length and penetrated the entire beam sections, representing those huge tensile forces progressed along the beam.

The cracking patterns for non-seismic assemblages are shown in Fig. 6 at the peak of the compression arch action, and in Fig. 7 at failure. For specimen S1, applying vertical displacement to the interior column generates flexural cracking through the compression arch action stage. The first crack occurred near the interior column at a load of 12.54 kN corresponding to 1.87 mm vertical displacement. Inclined cracks at the beam connection with the exterior columns are developed at a load level of 45.25kN with 5.86 mm deflection. With further increasing load, more cracks continued to arise while the previous ones propagated vertically toward the compression zones. After reaching the peak load of 69.57 kN, it was recorded that concrete crushing occurred in the zones of the beam assemblage subjected to excessive compression besides the interior column and at the bottom of the beams at both ends. When the vertical deflection was 65.12 mm, the vertical load began to ascend for the second time and this was credited to the catenary action developing in the beams. Also, the cracks were distrusted all over the beam length. Finally, at the collapse of specimen S1, the beam deflection dramatically increased to 96.07 mm and the top reinforcement ruptured closest to the exterior column.

To study the effect of existence concrete flanges on the behavior of the non-seismic specimens, the beam column assemblage of specimen S2 is considered. As shown in Fig[s]. 6.b and 7.b, the opening crack appeared at a load of 26.56 kN close to the interior column stub relating to 2.51 mm vertical deflection. As the vertical deflection increased to 9.66 mm; corresponding to vertical loading of 51.22 kN, more flexural cracks were formed in the beam span adjacent to the interior column. Inclined cracks at the beam-column joints at the exterior columns relating to a load level of 71.21 kN with 13.94 mm deflection were developed. Concrete crushing at the bottom of the

beams beside left and right exterior columns occurred at a maximum load level of 106.21 kN. When the displacement reached 100.38 mm, the vertical load began to rise again.

For specimen S3, the first crack was observed at the lower surface of the beam near the interior column at a load of 18.71 kN corresponding to 2.21 mm deflection. While the first crack occurred in the sections adjacent to the exterior columns was at a load of 42.1 kN with 5.22 mm deflection. Concrete splitting was observed at a displacement 14.75 mm relating to a peak load level of 75.23 kN. Compared to assemblage S1, more concrete crushing was noticed. When the vertical deflection was 59.06 mm, the vertical load began to climb again. Upon more increasing of the vertical deflection, the top rebar at the sections adjacent to the exterior columns fractured when the vertical displacement reached 101.27 mm and the test was terminated. The final failure mode of S3 is illustrated in Fig[s]. 6.c and 7.c. As shown in the figures, severe flexural cracks were observed through the beam span and beam ends differently from specimen S1.

Specimen S4 was designed to study the effect of bottom reinforcement ratios. Similar to S3, severe failure of S4 was also noticed at the middle joint region and at the beam ends. Fig[s]. 6.d and 7.d show that when S4 was at compression arch action stage, the first crack occurred near the interior column at a load of 20.65 kN corresponding to 2.46 mm vertical displacement. Higher load and deflections values were measured in comparison with specimen S1 as the bottom reinforcement ratios were increased. Inclined cracks at the beam connection with the exterior columns are developed at a load level of 57.1 kN with 8.82 mm deflection were developed.

After reaching the peak of compression arch action at load level of 82.46 kN, it was noticed that concrete crushing occurred at the zones of the beam assemblage subjected to excessive compression beside the interior column and at the bottom of the beam at both ends. When the vertical deflection was 80.16 mm, the vertical load began to ascend again, also the cracks were distrusted all over the beam length. At the end of the test, the catenary action was the dominant structural mechanism. Accordingly, cracks spread throughout the whole two-bay beam. Finally, at the collapse of specimen S4, the beam deflection dramatically increased to 104.62 mm and the test was terminated.

(a) S1

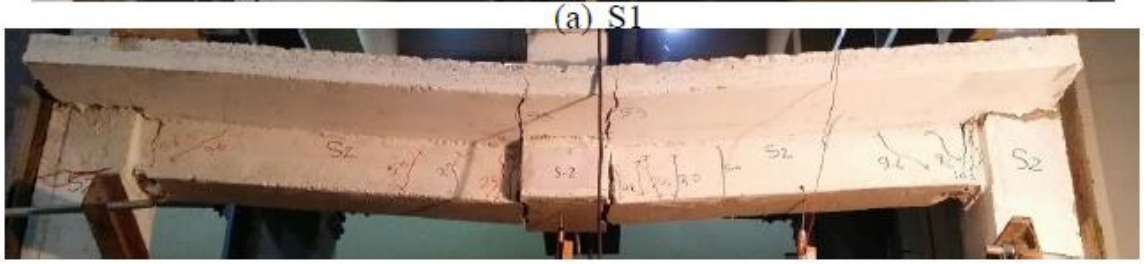

(b) S2

(c) S3

(d) S4

Figure 6: Crack patterns for non-seismic detailing of specimens at the peak of the compressive arch action.

(a) S1

(b) S2

(c) S3

(d) S4

Figure 7: Crack patterns for non-seismic detailing of specimens at the peak of the compressive arch action.

3.2 Observed Behavior and Failure Modes of Seismic Specimens

For the seismic specimens, there were no noticeable shear cracks developed in the beams during the test because of seismic detailing with much higher stirrups ratios in the plastic hinge zones. However, more severe flexural cracks appeared along the beam span compared to non-seismic specimens. Cracks were initiated through the compression arch action stage only as the catenary action stage was not be maintained through the test. The cracking patterns are shown in Fig. 8 at the peak of compression arch action, and in Fig. 9 at failure level.

During the testing of specimen S5, the onset crack appeared near the interior column at a load of 26.81 kN corresponding to 3.35 mm vertical displacement compared with a load level of 12.54 kN for S1. In Fig. 8.a, with the increase of vertical loads, more cracks appeared at the center of the two-bay beam. Inclined cracks were developed at the beam connection with the exterior columns at a load level of 62.21 kN with 8.77 mm displacement. When the deflection reached 54.14 mm, concrete crushing was observed at the middle and at the beam ends while concrete splitting occurred in the corner and middle joints at a displacement of 86.59 mm relating to a load level of 107.23 kN. With further increase in displacement, the concrete splitting became more severe as shown in Fig. 9. a. Top rebar at the beam ends and bottom rebar at the middle of the beam was fractured when the vertical displacement reached 146.96 mm and the test was stopped.

For specimen S6, which reflects the effect of continuity of bottom reinforcement in the two-bay beam without any lapping. Similar to S5, severe cracks were also concentrated at the middle joint region and at the beam ends. Fig. 8.b shows that when S6 was at compression arch action stage, the first crack occurred near the interior column at a load of 30.22 kN corresponding to 3.65 mm vertical deflection. Higher load and deflections values compared with specimen S5 were obtained. Inclined cracks at the beam-column connection at the exterior columns relating to a load level of 65.14 kN with 10.69 mm deflection were developed. After reaching the peak of compression arch action at a load level of 120.91 kN, it was noticed that concrete splitting occurred in the zones of the beam assemblage subjected to excessive tensions besides the interior column and at the bottom of the beams at both ends. When the vertical deflection reached 85.51 mm the concrete crushing was observed at the middle and beam ends. Finally, at the collapse of specimen S6, the beam deflection dramatically increased to 149.10 mm and the test was stopped as shown in Fig. 9. b.

(a) S5

(b) S6

(c) S7

Figure 8: Crack Patterns for seismic specimens at the peak of the compressive arch action.

The behavior of specimen S7 was different from the preceding seismic specimens due to the existence of flanges over the span of the two-bay beam. The first main cracks occurred during the test were at the right and at the left of the interior column stub initiated at the bottom surface of the beam and propagated vertically at a load level of 39.23 kN and at a displacement of 4.65 mm. The inclined cracks were adjacent to the face of the right and the left exterior columns, and initiated at the top concrete surface at a load level of 87.73 kN and a vertical deflection of 7.49 mm. The first crack observed in the flange was recorded at a load of 45.23 kN adjacent to the interior column stub. Under further loading, concrete crushing in the bottom of the beam beside left and right columns at a maximum load level of 156.92 kN. When the displacement reached 98.07 mm, the vertical load began to decline. By the end of the test, the vertical and inclined cracks became wider and penetrated towards the compression zone, and the beam deflection dramatically increased to 152.12 mm and the test was stopped. Figures. 8.c and 9.c show the crack pattern of specimen S7.

In order to explore the effect of seismic detailing on the response of the beam-column assemblages, crack patterns and failure modes of non-seismic specimens, S1 and S2 were compared to seismic specimens S5 and S7. For assemblage S5, the use of seismic detailing leads to increase in the first crack load by 18.1%, also the inclined crack load at the beam connection with the exterior column is increased by 37.5% compared to specimen S1. For specimen S7, the application of seismic detailing in addition to concrete slab leads to improve the cracking loads. For the onset-cracking load, the increase factor is 1.47 times. For the inclined crack load at the beam joint with the external column, the increase factor is 1.23 times compared to specimen S1. The test results indicated that the use of seismic detailing had a significant contribution to both onset-cracking resistance and failure modes of the assemblages under interior column loss.

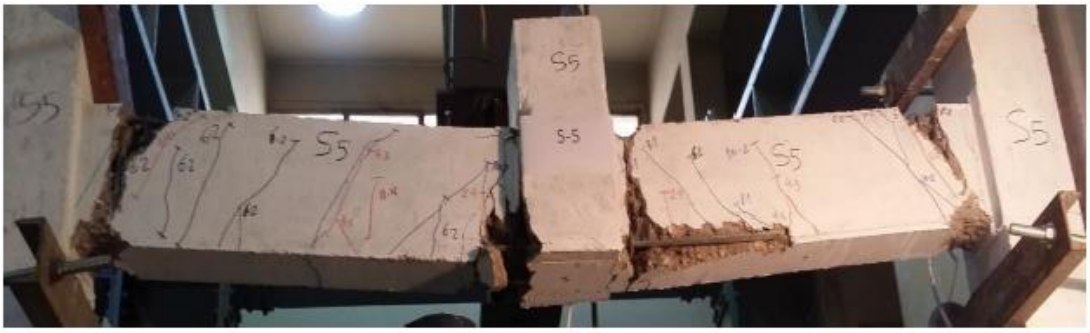

(a) S5

(b) S6

(c) S7

Figure 9: Crack patterns for seismic detailing specimens at failure.

3.3 Load-Displacement Behavior of Non-Seismic Specimens

The results of all beam-column assemblages could be clarified together by the identification of six displacements levels and the corresponding loads as summarized by Qian et al. [14]. The chosen displacement levels and associated loads are as follows:

1) the cracking displacement (Δ_{crs}) at which the onset-cracking load (P_{crs}) is reached;

2) Yield deflection (Δ_y) at which the yield load (P_y) is achieved where the tension steel yielded;

3) The ultimate displacement (Δ_u) at which the ultimate resistant capability (P_u) is realized;

4) (Δ_{nf}) is the vertical deflection near collapse phase (P_{nf}), which corresponded to a 25 % reduction in the maximum ability on the descending branch of the load-deflection curve;

5) (Δ_{ct}) is the vertical displacement at which the catenary action initiated (P_{ct}), where the slope of the reduction of force resistance reformed extensively; and

6) The straight down deflection (Δ_f) at the final collapse stage (P_f), which was expressed as the point when the force resistance completely disappears. A summary of the major experimental outputs for all beam-column assemblages are detailed in Tables 3 and 4.

Table 3: Summary of experimental loads results.

Specimen	Initial Cracking Load P_{crs} (kN)	Yield Load, P_y (kN)	Peak (Ultimate) Load, P_u(kN)	Near Collapse Load, P_{nf} (kN)	Catenary Load, P_{ct} (kN)	Failure Load, P_f (kN)
S1	12.54	55.65	69.57	52.17	45.25	55.71
S2	26.56	94.96	106.21	79.65	69.87	80.23
S3	18.71	59.89	75.23	56.42	44.90	52.17
S4	20.65	66.12	82.46	61.84	45.23	64.97
S5	26.81	85.81	108.32	81.24	----	64.51
S6	30.22	78.34	120.91	90.68	----	71.81
S7	39.23	125.53	156.92	117.69	----	95.13

P_{nf} = **0.75 *P_u**

Table 4: Summary of the measured displacements.

Specimen	Δ_{crs}**(mm)**	Δ_y**(mm)**	Δ_u **(mm)**	Δ_{nf} **(mm)**	Δ_{ct} **(mm)**	Δ_f **(mm)**	μ_Δ Δ_{nf} / Δ_y
S1	1.87	9.53	15.62	23.41	65.12	96.07	2.45
S2	2.51	16.57	66.23	85.31	100.38	107.23	5.14
S3	2.21	9.35	14.75	21.77	59.06	101.27	2.33
S4	2.46	10.54	18.97	22.81	80.16	104.62	2.16
S5	3.35	17.19	50.49	138.23	----	146.96	8.04
S6	3.65	15.83	52.91	100.52	----	149.1	6.35
S7	4.65	13.05	88.13	135.65	----	152.12	10.31

Figure 10 shows the load-deflection correlation for all non-seismic specimens. For specimen S1, it can be observed that primarily, there is a linear connection between the applied load and the straight down displacement. The onset-cracking load P_{crs} was 12.54 kN corresponding to a displacement Δ_{crs} of 1.87 mm. First reinforcement yielding developed at the mid-span of the two-bay beam due to positive bending moments and then at the exterior columns due to negative bending moments. The yield load P_y 55.65 kN was achieved at a deflection Δ_y of 9.53 mm. Sequentially, the displacement increased significantly with a slight enhancement in load capacity. By the end of compression arch action stage, the beam mid-span displacement reached 15.62 mm and S1 attained the ultimate resistant capability Pu 69.57 kN. The sharp drops in the load-displacement diagrams are due to the crushing of concrete and the rupture of reinforcement bars. The peak capacity dropped by 25 % when the displacement Δ_{nf} reached 23.41 mm. The catenary action stage took place when the displacement Δ_{ct} achieved 65.12 mm. The load resistance was increasing slowly with increasing displacement until the final displacement Δ_f reached 96.07 mm corresponding to a final collapse load $P_{f\ of}$ 55.71 kN.

For assemblage S2, the start-cracking load P_{crs} was 26.56 kN paralleling to a displacement Δ_{crs} of 2.51 mm. The specimen started to yield at the displacement Δ_y of 16.57 mm and a yield load P_y 94.96 kN. Consecutively, the displacement increased significantly with a slight enhance in the load capacity. By the end of the compression arch action stage, the beam mid-span displacement reached 66. 23 mm and S2 attained the ultimate resistant capacity Pu 106.21 kN, which is 152.67 % of the S1 peak load. The compression arch action capacity of S2 was greater than that of S1, this indicates that the concrete slab has a considerable enhancement to the structural resistance. Specimen S2 peak capacity was

almost remained constant up to a displacement level of 69.71 mm then dropped by 25 % when the displacement Δ_{nf} reached 85.31 mm. The catenary action stage took place when the displacement Δ_{ct} achieved 100.38 mm. The load resistance was increasing slowly with increasing displacement until the final displacement Δ_f reached 107.23 mm corresponding to a final failure load P_f of 80.23 kN, which is 44 % larger than S1 failure load. For assemblage S3, in which the increase of bottom reinforcement ratio was 44.8%. The onset cracking force P_{crs} was 18.71 kN corresponding to a displacement Δ_{crs} of 2.21 mm as shown in Fig. 10. First reinforcement yielding developed at the mid-span of the two-bay. The yield load P_y 59.89 kN was reached at a displacement Δ_y of 9.35 mm. Assemblage S3 achieved the ultimate resistant capacity Pu 75.23 kN, which is 108.13 % of that for S1 peak load. The catenary action stage happened when the displacement Δ_{ct} achieved 59.06 mm. The load resistance was increasing with increasing displacement. The load capacity enhancement was higher than that of S1. The middle joint displacement reached 84.68 mm corresponding to a load of 67.51 kN, which is 31.82 % larger than S1. The final displacement Δ_f reached 101.27 mm corresponding to a final failure load P_f of 52.17 kN.

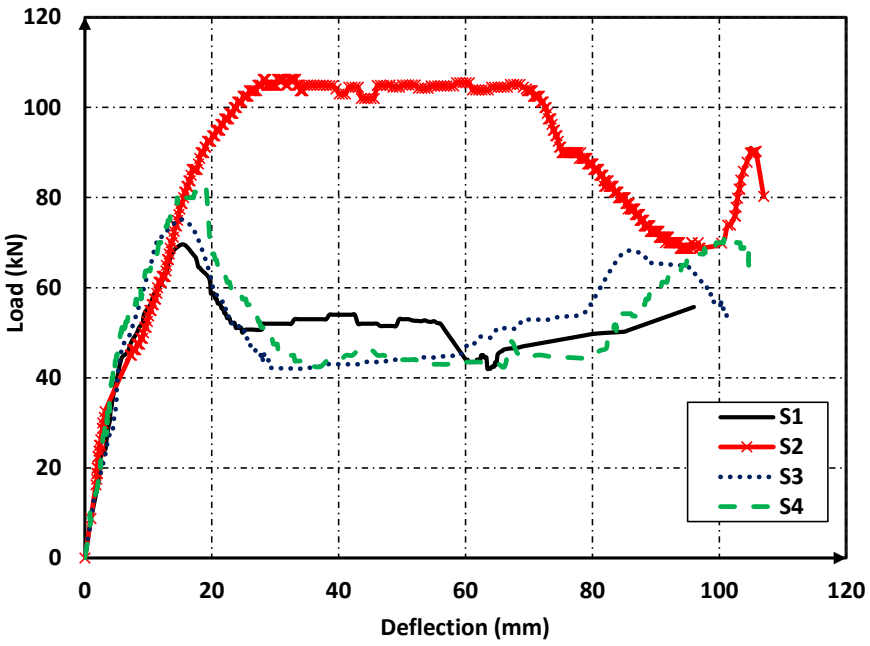

Figure 10: Load- deflection curves for specimen S1, S2, S3, and S4 (specimens with non-seismic detailing).

For specimen S4, the specimen developed two stages of alternative load path containing compression arch action, and catenary action. The response of S4 was the same as S1 from starting loading to the peak capacity then the strength of S4 reduced rapidly compared to S1. The onset cracking force P_{crs} was 20.65 kN corresponding to a displacement Δ_{crs} of 2.46 mm. First reinforcement yielding developed at the mid-span of the two-bay, the yield load P_y 66.12 kN was reached at a displacement

Δ_y of 10.54 mm. By the end of the compression arch action stage, the beam displacement reached 18.97 mm and S4 achieved the ultimate resistant capacity P_u 82.46 kN, which is 118.52 % of the S1 peak load. As displacement increased, the vertical load decreased and started to increase again at a displacement Δ_{ct} of 80.16 mm, which corresponded to a vertical load P_{ct} of 45.23 kN. The load resistance was increasing slowly with increasing displacement until the final displacement Δ_f reached 104.62 mm corresponding to a final failure load P_f of 64.97 kN, which is 15.79 % larger than S1 failure load.

3.4 Load-Displacement Behavior of Seismic Specimens

For the seismic specimens, Fig. 11 shows the applied force versus downward deflection relationship of specimen S5, S6, and S7. For assemblage S5, the simulated collapse of the interior column along with the increase in the vertical deflection may be divided into four stages. The first stage can be counted as the elastic stage with initial cracking force P_{crs} of 26.81 kN and a displacement Δ_{crs} of 3.35 mm. The second stage is the onset of the inelastic behaviour. The yield load P_y 85.81 kN was achieved at a deflection Δ_y of 17.19 mm. It is observed that most of the reinforcement bars yielded at the mid-span of the two-bay beam and then at the exterior columns, indicating the formation of plastic hinges at the end of this stage. Stage three is the end of the compression arch action stage where the vertical displacement increases to 50.49 mm and S5 attained the ultimate resistant capability P_u 108.32 kN. Specimen S5 peak capacity was almost remained constant up to a displacement level of 98.23 mm. The deformations are governed by plastic rotations of the beam ends and severe concrete crushing was observed as the vertical displacement increased. The peak capacity dropped by 25 % when the displacement Δ_{nf} reached 138.23 mm. Catenary action stage was not achieved at the test as the limitations of LVDT deflections. The load resistance was decreasing slowly with increasing displacement until the final displacement Δ_f reached 146.96 mm corresponding to a final collapse load P_f of 64.51 kN.

In order to investigate the effect of bars layout on the collapse resistance, the bottom reinforcement layer of specimen S6 was continued through the two-bay beam span without lapping. The behaviour of S6 is similar to S5 as follows; the initial cracking force was P_{crs} of 30.22 kN anticipated with a displacement Δ_{crs} of 3.65 mm. The yield load P_y 78.34 kN was achieved at a deflection Δ_y of 15.38 mm. The ultimate resistant capacity was P_u 120.91 kN, which is 111.62 % of S5 peak load. The compression arch action capacity of S6 was greater than that of S5. This indicates that the continuity of bottom reinforcement has a slight enhancement to the structural resistance. The final displacement Δ_f reached 149.1 mm corresponding to a final failure load P_f of 71.81 kN, 11.3 % larger than S5 failure load.

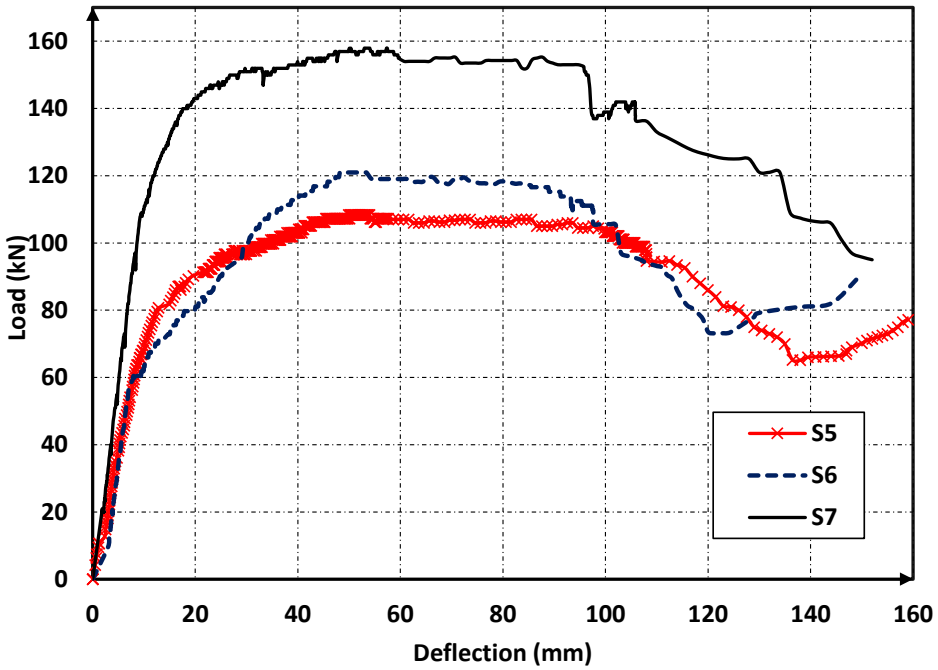

Figure 11: Load-deflection curves for specimen S5, S6, and S7 (specimens with seismic detailing).

For assemblage S7, the initial cracking force P_{crs} was 39.23 kN paralleling to a displacement Δ_{crs} of 4.65 mm. The specimen started to yield at a displacement Δ_y of 13.05 mm and a yield load P_y 125.53 kN Consecutively. The displacement increased significantly with a slight enhance in load capacity. By the end of the compression arch action stage, the beam mid-span displacement reached 88.13 mm and S7 attained the ultimate resistant capacity P_u 156.92 kN, which is 144.86 % of S5 peak load. The compression arch action capacity of S7 was greater than that of S5. This indicates that the concrete slab has a considerable enhancement to the structural resistance. Specimen S7 peak capacity was almost remained constant up to a displacement level of 95.63 mm then dropped by 25 % when the displacement Δ_{nf} reached 135.65 mm. The Catenary action stage couldn't be activated as mentioned before. The load resistance was decreasing slowly with increasing displacement until the final displacement Δ_f reached 152.12 mm corresponding to a final failure load P_f of 95.13 kN, which is 47.46 % larger than S5 failure load.

4 ANALYSIS OF THE REST RESULTS

4.1 Displacement Ductility

Ductility is defined as the capability of the reinforced concrete elements to displace in elastic form through numerous cycles of deformations without large degradation in strength or stiffness [13 and 14]. In the case of the strength or stiffness extremely decayed, the deflections significantly increased beyond elastic limits, and the structure may break down. Mathematically, ductility is usually presented by the ratio of maximum displacement at a given level to displacement at yielding of tension reinforcement. The maximum displacement expected during the design-level is Δ_{nf}, which corresponds to a 25 % reduction in the maximum ability on the descending branch of the load-deflection curve, [13]. The displacement ductility factor is given by;

$$\mu_{\Delta} = \frac{\Delta_{nf}}{\Delta_{y}} \quad (1)$$

Figure 12 and Table 4 outline the displacement ductility factors μ_{Δ} of the tested beam-column assemblages. For the non-seismic specimens, the ductility factors of S1, S2, S3, and S4 are 2.45, 5.14, 2.33, and 2.16 respectively. S2 ductility level is increased by 110% compared with that of S1 due to the contribution of concrete flanges attached to the assemblage all over the span. For specimen S3, the ductility level is almost the same compared with S1 due to the same tension bottom reinforcement configuration. For assemblage S4, the ductility factor is decreased by 11.8% compared with S1 due to the increase in bottom reinforcement ratio which leads to delay the yielding displacement of tension reinforcement.

For the seismic specimens, the ductility factors of S5, S6, and S7 are 8.04, 6.35, and 10.31 respectively. S7 ductility level is increased by 28.23 % compared with that of specimens S5 due to the influence of concrete flanges attached to the specimen. For assemblage S6, the ductility factor is decreased by 21.1 % compared with that of S5 due to the continuity of bottom reinforcement. In order to investigate the effect of seismic detailing on the displacement ductility factor of the beam-column assemblages, non-seismic specimens S1 and S2 were compared to seismic detailing assemblages S5 and S7. The ductility factor is significantly enhanced by using the seismic detailing provisions. The displacement ductility factor is increased to 3.28 and 2.01 times for assemblages S5 and S7, respectively, compared with S1 and S2.

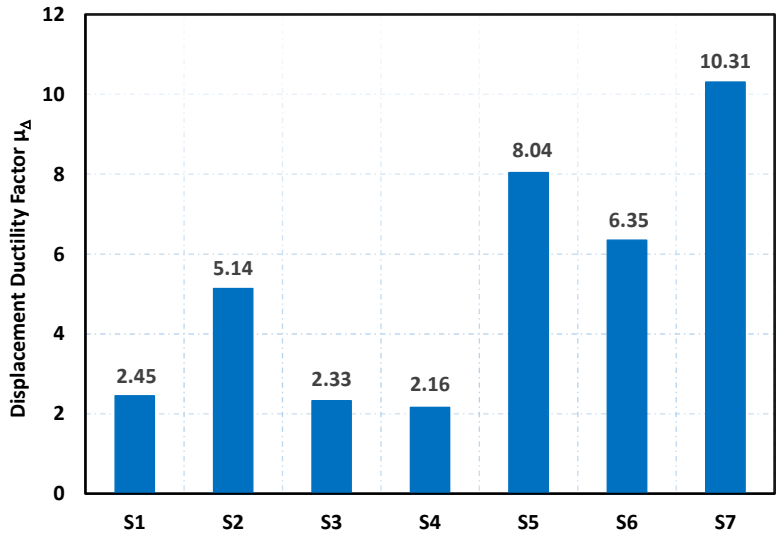

Figure 12: Displacement ductility factor (μ_Δ) of the tested assemblages.

4.2 Energy Absorption

In the situation where a column is excluded due to severe damage or explosion, the load resisted by the missing column loses its potential energy which must be transferred to the remaining structural elements as internal energy. Absorbing energy is extensively needed for the reinforced concrete structures to withstand progressive collapse and to stop the local collapse from distribution throughout the structure. The absorbed energy by the beam-column assemblage during the test is calculated as the area under the load-deflection curve. The energy dissipation capacity is given for m load steps as;

$$E_n = \sum_{i=1}^{m} (P_i \, \Delta_i) \qquad (2)$$

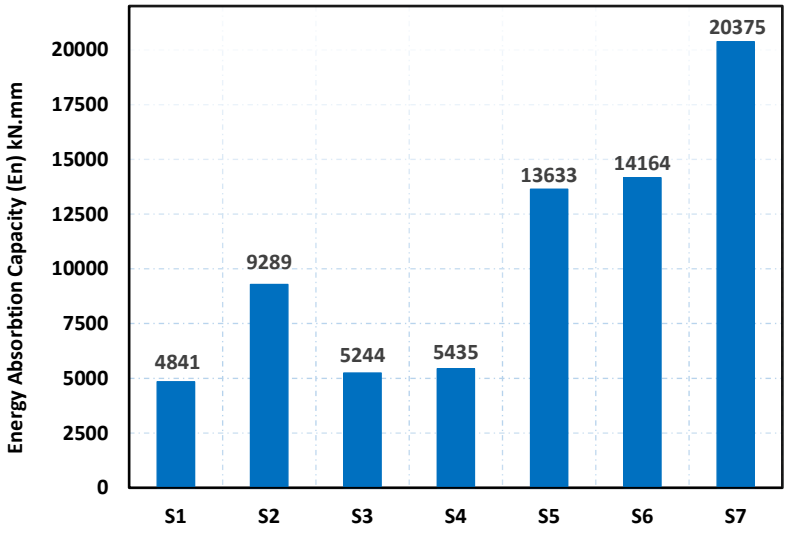

Figure 13: Energy absorption capacity (E_n) of the tested assemblages.

Figure 13 presents the capacity of the absorbed energy of the tested specimens. For the non-seismic specimens, the over-all energy dissipated for specimens S1, S2, S3 and S4 are 4.8 kN.m, 9.2 kN.m, 5.2 kN.m, and 5.4 kN.m respectively, at the end of each test. For assemblage S2, the energy dissipation capacity is increased by 91 % compared with that of S1 due to the existence of concrete flanges. For S3 and S4, the energy dissipation capacity is increased slightly by 8.30 % and 12.30 % compared with S1 due to the increase in the top and bottom reinforcement ratios. The total energy absorbed for seismic assemblages S5, S6 and S7 are 13.6 kN.m, 14.1 kN.m, and 20.3 kN.m respectively, at the end of each investigation. For specimen S7, the energy absorption ability is increased by 49.5 % compared with that of S5 due to the effect of concrete flanges. For assemblage S6, the energy dissipation capacity is increased by 3.90 % compared with S5 due to the effect of bottom reinforcement continuity without lapping at beam mid-span. The energy absorption ability is considerably improved by utilizing the seismic detailing provisions. The energy absorption factor increased by 2.83 and 2.21 times for assemblages S5 and S7, respectively compared with the non-seismic assemblages S1 and S2. Therefore, appropriate internal energy dissipation is supplied through enough ductility, continuity of rebars, seismic detailing provisions, and redundancy which leads to decrease the progressive collapse damage to the structures.

4.3 Contribution of Compression Arch Action

As stated in the existing studies [15 - 17], the Compression Arch Action (CAA) has been observed to enhance significantly the assemblage structural capacity. Therefore, the contribution of (CAA) for both non-seismic and seismic specimens are assessed in terms of peak ultimate loads. From Table 3, the compressive arch action load of non-seismic specimens S1, S2, S3, and S4 are 69.57 kN, 106.21 kN, 75.23 kN, and 82.46 kN respectively. For S2, the ultimate load is increased by 53 % compared with that of S1, due to the existence of concrete slabs which lead to expanding the compressive concrete zone then enhancing the assemblage internal carrying capacity. For S3, the peak load is increased by 8.0 % compared with S1, due to increasing top reinforcement ratios at beam-ends which lead to an equinoctial enhancement to the arch resistance. For Assemblage S4, the maximum load is increased by 18.5 % compared with that of S1, as a result of increasing mid-span bottom reinforcement which leads to an increase in the tension reinforcement. The enhancement of bottom reinforcement had a noticeable improvement on the compression arch capacity. For seismic specimens, the maximum compressive arch action load of S5, S6, and S7 are 108.32 kN, 120.91 kN, and 156.92 kN respectively. For S6, the peak load is increased by 11.60 % compared with S5, because of the continuity of the

bottom reinforcement without lapping at the interior column. For Assemblage S7, the ultimate load is increased by 49 % compared with that of S5, due to the existence of concrete flange. For assemblage S5, the using of seismic detailing leads to an increase in the peak arching load by 55% compared with non-seismic assemblage S1. For specimen S7, the utilizing of seismic detailing in addition to concrete slab leads to improve the ultimate arching loads, the load increase is 47% compared with specimen S2.

Experimental results showed that the contribution of compressive arch action to the successive collapse resistance is affected by the addition of concrete flanges, seismic detailing, continuity of the bottom reinforcement, top and bottom tension reinforcement. Referring to Fig[s]. 10 and 11, it is obvious that there is a variation in the maintaining of peak arching capacity for all specimens. The non-seismic assemblages S1, S3, and S4 reached the maximum arching capacity at a deflection/span ratio (Δ/L) 1.00% of the two-span beam length, and then there was a breakdown in the arching capacity. On the other hand, for assemblage S2, the ultimate arching capacity was reached at a deflection/span ratio 1.30% of the two-bay beam span. The addition of concrete slabs of S2 helped to mitigate the degradation of arching peak capacity from a deflection/span ratio corresponding to 1.30% to 3.30% of the beam span. For the seismic specimens S5, S6, and S7 reached the maximum arching capacity at a deflection/span ratio 2.50% of the two-span beam length. The seismic detailing and addition of concrete slabs for assemblages S5, S6, and S7 helped in keeping of peak arching capacity without any degradation from a deflection/span ratio corresponding to 2.50% to 4.30% of the beam length. Laboratory results showed that the addition of concrete slabs and seismic detailing had a great enhancement in maintaining of beam-column assemblages peak arching capacity.

4.4 Activation of Catenary Action

The catenary action is the main capability that is needed to help a damaged structure to maintain an alternative balance arrangement. The term of catenary action can be defined as the ability of reinforced concrete beams to develop huge deformations such that external loads are mainly endured by the axial tension forces that progress in the beams, i.e., catenary forces, Yu et al. [18]. Under such situations, the beams are not capable of resisting the externally applied loads through flexural action only and demand additional resistance through activation of the catenary mechanism. Through the tests, after bottom steel reinforcement yielding, a transition point developed in each curve, the cracks propagate quickly and the concrete which could afford compressive stress is reduced. The beam-column assemblage switched from the arch action stage to the catenary action stage. Axial tension forces in the beam are developed instead of compression ones. When the cracks developed to the entire

beam depth, the applied load on beam-column assemblage was completely sustained by the steel reinforcement. The experimental results showed that the specimens; S1, S2, S3, and S4 were able to produce catenary action, however the seismic specimens; S5, S6, and S7, failed to develop catenary action due to lab limitations of the LVDT capacity.

4.5 Comparative Studies with Existing Models

In order to ensure further verification of the beam-column assemblage experimental results, the results were evaluated using some existing models. The peak compression arch action capacity has been evaluated by Park [19] and Mohajeri [20] models. Table 5 outlines the calculated ratios of the experimental arching capacity $P_{u\ exp}$. and the theoretical arching capacity P_u for the two models. The average ratio of the laboratory and the model's predictions are 1.05 and 1.10 for Park [19] and Mohajeri [20], respectively. The standard deviation for Park [19] model is 0.24 and is 0.16 for Mohajeri [20] model. Meany recent reaches studied progressive collapse experimentally, numerically and analytically [21-26]. Through the comparison, it is clear that the laboratory results are close to the proposed analytical results by the two models. This is a good indicator of the laboratory tests carried out on the beam-column assemblages under the influence of all testing variables.

Table 5: Predictions of the compression arch action.

Specimen No.	Reinforcement details	P_u Exp.	P_u Park. [19]	P_u Mohajeri [20]	P_u Exp. / P_u Park [19]	P_u Exp. / P_u Mohajeri[20]	Energy Absorption Capacity (E_n)
		(kN)	(kN)	(kN)			(kN.mm)
S1	Non-Seismic	69.57	75.7	70.4	0.92	0.99	4841
S2	Non-Seismic	106.21	74.2	78.8	1.43	1.35	9289
S3	Non-Seismic	75.23	86.8	78.5	0.87	0.96	5244
S4	Non-Seismic	82.46	88.1	78.5	0.94	1.05	5435
S5	Seismic	108.32	123.5	110.4	0.88	0.98	13633
S6	Seismic	120.91	123.5	110.4	0.98	1.09	14164
S7	Seismic	156.92	115.3	122.2	1.36	1.28	20375
				Average	1.05	1.10	
				STD	0.24	0.16	

Where: STD is the stander deviation**.**

CONCLUSION

1- The failure mode for all specimens was dominated by flexure action. The formation of large cracking in addition to concrete crushing was concentrated at the beam connections with the eliminated interior column and with the exterior columns. The use of seismic detailing in terms of stirrups spacing, top reinforcement ratios, and bottom reinforcement extensions of bars had a significant enhancement to the assemblage onset-cracking resistance along with the delaying the assemblage final collapse deflections.

2- The results of the non-seismic specimens indicated that the addition of concrete flanges had a considerable contribution to both ultimate and failure capacity resistance. The peak and failure capacities of assemblage S2 were 52% and 44% greater than S1, respectively. Increasing top reinforcement at upper critical sections by 45% had a small enhancement of peak load capacity and collapse resistance. The enhancement factor is 8% of assemblage S3 compared with S1. Increasing bottom reinforcement by 45% along beam span had a moderate contribution to both ultimate and failure capacity resistance. The increasing factor of specimens S4 is 18% larger than S1.

3- The seismic detailing and provisions had a considerable contribution to both ultimate and failure capacity resistance of the assemblages with and without considering the slabs effect. The peak load of specimens S5, S7 was 56%, 47% greater than S1, and S2, respectively. The continuity of bottom reinforcement without any lapping along the beam span had a small enhancement of the peak load capacity and the collapse resistance. The increasing factor for assemblage S6 is 11% for both peak and failure capacities compared to S5.

4- Appropriate internal energy dissipation is supplied through enough ductility, continuity of re-bars, seismic detailing provisions, and redundancy which leads to decrease the progressive collapse damage of the structures. The ductility factor is significantly enhanced by using the seismic detailing provisions. The increase factor is 3.28 and 2.01 for assemblages S5 and S7, compared to S1 and S2, respectively. At the same time, the energy absorption ability is considerably improved by utilizing the seismic detailing provisions. The increase factor is 2.83 and 2.21 for assemblages S5 and S7, respectively compared to the non-seismic assemblages S1 and S2.

5- The addition of concrete flanges and seismic detailing had a great enhancement in maintaining of beam-column assemblages peak arching capacity without sudden break-down. The seismic detailing and the addition of concrete slabs for assemblages for specimens S5, S6, and S7 helped in keeping of the peak arching capacity without any degradation from a displacement corresponding to 2.50 % (1/40) up to 4.30 % (1/83) of the beam length.

REFERENCES

[1] American Society of Civil Engineers (ASCE), (2010), "Minimum Design Loads for Buildings and other Structures", ASCE/SEI 7-10, Reston, VA.

[2] Department of Defence (DoD), (2016),"Design of Structures to Resist Progressive Collapse", Unified Facility Criteria, UFC 4-023-03, Washington, DC.

[3] General Services Administration (GSA), (2016)," Alternate Path Analysis and Design Guidelines for Progressive Collapse Resistance", Washington, DC.

[4] Farhang, V. N., Valipour, H, Samali B, and Foster, S., , (2013), "Development of Arching Action in Longitudinally-Restrained Reinforced Concrete Beams", Construction Build Material;47:7–19.

[5] Yu J., and Tan KH. , (2013), "Special Detailing Techniques to Improve Structural Resistance Against Progressive Collapse", Journal of Structural Engineering .2013;140(3):04013077.

[6] Tsai, M. H., and Chang, Y. T. ,(2015), "Collapse-Resistant Performance of RC Beam–Column Sub-Assemblages with Varied Section Depth and Stirrup Spacing", The Structural Design of Tall and Special Buildings, 24(8), 555-570.

[7] Pour, H. V., Vessali, N., Foster, S. J., and Samali, B., (2015)," Influence of Concrete Compressive Strength on the Arching Behaviour of Reinforced Concrete Beam Assemblages", Advances in Structural Engineering, 18(8), 1199-1214.

[8] Choi, H., and Kim, J. ,(2011)," Progressive Collapse-Resisting Capacity of RC Beam–Column Sub-Assemblage", Magazine of Concrete Research, 63(4), 297-310.

[9] Ren, P.Q., Li, Y., Lu, X.Z, Guan, H. and Zhou Y.L., , (2016), "'Experimental Investigation of Progressive Collapse Resistance of One-Way Reinforced Concrete Beam-Slab Substructures under a Middle-Column-Removal Scenario", Engineering Structure 118:28–40.

[10] Lu, X.Z., Lin, K.Q., Li, Y., Guan, H., Ren, P.Q., and Zhou, Y.L., , (2017),"Experimental Investigation of RC Beam-Slab Substructures Against Progressive Collapse Subject to an Edge-Column Removal Scenario", Engineering Structure, 149:91–103.

[11] Egyptian Code of Practice: ECP 203-(2017), "Design and Construction for Reinforced Concrete Structures", Ministry of Building Construction, Research Center for Housing, Building and Physical Planning, Cairo, Egypt.

[12] Egyptian Code of Practice: ECP 201-(2012), “Egyptian Code for Calculating Loads and Forces in Structural Work and Masonry” , Ministry of Building Construction, Research Center for Housing, Building and Physical Planning, Cairo, Egypt.

[13] ACI Committee 318M-11, , (2011), “Building Code Requirements for Structural Concrete”, American Concrete Institute, Detroit, Michigan, Farmington Hills, USA.

[14] Qian, K. and Li, B., , (2012)," Slab Effects on Response of Reinforced Concrete Substructures after Loss of Corner Column", ACI Structure Journal 109(6):845–855.

[15] Park, R., (1989),"Evaluation of Ductility of Structures and Structural Assemblages from Laboratory Testing", Bull. N.Z. Nat. Soc. Earthquake Engineering 22 - 155–166.

[16] Qian, K., Li, B., and Ma. J.X., , (2015)," Load-Carrying Mechanism to Resist Progressive Collapse of RC Buildings", Journal of Structural Engineering;141(2):04014107.

[17] Su, YP, Tian Y, and Song X, , (2009)," Progressive Collapse Resistance of Axially-Restrained Frame Beams", ACI Structural Journal;106(5):600–7.

[18] Yu, J., and Tan, K.H., , (2013),"Experimental and Numerical Investigation on Progressive Collapse Resistance of Reinforced Concrete Beam Column Sub-Assemblages", Engineering Structure;55:90–106.

[19] Park, R., Gamble, W.L., , (2000),"Reinforced Concrete Slabs", John Wiley and Sons.

[20] Mohajeri, N. F., Usefi, N., and Abbasnia, R., (2018),” Analytical Investigation of Reinforced Concrete Frames under Middle Column Removal Scenario”, Advances in Structural Engineering, 21(9), 1388-1401.

[21] Bigonah, M., Soltani, H., Zabihi, S., M., and Shyanfar, M. A., (2020),” Performance Evaluation on Effects of All Types of Infill Against the Progressive Collapse of Reinforced Concrete Frames”, Asian Journal of Civil Engineering, 21(3), 395-409.

[22] Chen, W., Lin, B., Li, D., Zhang, J., and Cui, S., (2022),” Progressive Collapse Performance of Shear Strengthened RC Frames by NANO CFRP”, Nanotechnology Reviews, 11(1), 811-823.

[23] Guo, X., Yang, Z., Li, Y., Guan, H., Lu, X., & Diao, M. (2022). Progressive Collapse of Flat Plate Substructures Initiated by Upward and Downward Punching Shear Failures of Interior Slab–Column Joints. Journal of Structural Engineering, 148(2), 04021262.

[24] Qin, W., Liu, X., Xi, Z., Huang, Z., Al-Mansour, A., and Fernand, M., (2021),” Experimental Research on the Progressive Collapse Resistance of Concrete Beam-Column Sub-Assemblages Reinforced with Steel-FRP Composite Bar”, Engineering Structures, 233, 111776.

[25] Vinay, M., Rao, P. K. R., Dey, S., Swaroop, A. H. L., Sreenivasulu, A., and Rao, K. V., (2022),” Evaluation of Progressive Collapse Behavior in Reinforced Concrete Buildings”, Structures, Vol. 45, pp. 1902-1919.

[26] Scalvenzi, M., Gargiulo, S., Freddi, F., and Parisi, F., (2022),” Impact of Seismic Retrofitting on Progressive Collapse Resistance of RC Frame Structures”, Engineering Failure Analysis, 131, 105840.